Experimental results for hydrocarbon refrigerant vaporization in brazed plate heat exchangers at high pressure

Adriano Desideri[1*], Martin Ryhl Kærn[2], Torben Schmidt Ommen[2], Jorrit Wronski[3],Sylvain Quoilin[1], Vincent Lemort[1], Fredrik Haglind[2]

[1] University of Liege, Thermodynamics laboratory,
Liege, Belgium
adesideri@ulg.ac.be, squoilin@ulg.ac.be, vincent.lemort@ulg.ac.be

[2] Technical University of Denmark, Thermal energy systems,
Kongens Lyngby, Denmark
tsom@mek.dtu.dk, frh@mek.dtu.dk

[3] IPU,
Kongens Lyngby, Denmark
jowr@ipu.dk
* Corresponding Author

ABSTRACT

In recent years the interest in small capacity organic Rankine cycle (ORC) power systems for harvesting low quality waste thermal energy from industrial processes has been steadily growing. Micro ORC systems are normally equipped with brazed plate heat exchangers which allows for efficient heat transfer with a compact design. An accurate prediction of the heat transfer process characterizing these devices is required from the design phase to the development of model-based control strategies. The current literature is lacking experimental data and validated correlations for vaporization of organic fluids at typical working conditions of ORC systems for low temperature waste heat recovery (WHR) applications. Based on these premises, a novel test-rig has been recently designed and built at the Technical University of Denmark to simulate the evaporating condition occurring in a small capacity ORC power unit.
In this contribution the preliminary experimental results obtained from the first experimental campaign carried out on the rig are reported. HFC-134a was selected as working fluid. The experiments were carried out at saturation temperature of 60, 70 and 80 °C and inlet and outlet qualities ranging between 0.01-0.3 and 0.5-0.95 respectively. The heat flux ranged between 19.4 and 43.1 kWm^{-2}. The results are presented in terms of refrigerant side heat transfer coefficient and pressure drop.
The heat transfer coefficient showed significant sensitivity to the saturation temperature and was characterized by a decreasing trend with respect to the mean evaporator quality.
The frictional pressure drop showed a linear dependence on the mean quality value and increased as the saturation temperature decreased. The experimental heat transfer coefficients were compared with a well-known correlation for nucleate boiling which is able to predict the results with an accuracy of around 20 %.

1. INTRODUCTION

In recent years, there has been an increasing interest in investigating low temperature small capacity (tens of kW_{el}) organic Rankine cycle (ORC) power systems (Walraven & D haeseleer, 2013)(Declaye, Quoilin, Guillaume, & Lemort, 2013)(Quoilin, van den Broek, Declaye, Dewallef, & Lemort, 2013). ORC units have been proven to be a mature and viable technology in the large capacity range (Angelino et al., 1994)(Angelino, Gaia, & Macchi, 1984) and are expected to play a major role in recovering the vast amount of low temperature thermal energy available in industrial processes (IEA, 2010) (Prasad, 1980) (Verneau, 1979).
Due to the non-constant nature of the wasted thermal energy available from industrial facilities, specific control strategy ensuring safe and optimal operation of the ORC unit in any conditions are required. Before a control system can be designed the dynamic behaviour of the ORC unit needs to be well investigated. Small capacity ORC systems are

characterized by very different dynamics compared to larger power plants. In particular due to the small size of the components the main system dynamics are related to the thermal inertia of the heat exchangers which are often of the brazed plate type (BPHX) (Desideri et al., 2016) (Quoilin, October 2011). In an ORC power unit, the evaporator is considered the most critical heat transfer component. Ensuring good heat transfer in the evaporator allows reducing entropy production leading to higher expander inlet temperature and thus better system efficiency. Accurate evaporation heat transfer correlations are therefore required from the early design stage to the development and testing of efficient model-based control strategies.

Despite the broad use of BPHXs for small ORC systems, the available literature covering the performance of BPHXs at typical evaporating temperatures and pressures of ORC power units for low quality WHR is scarce. Most of the available correlations are derived from water-based experiments (Muley & Manglik, 1999) (Palm & Claesson, 2006) and are not validated in the typical temperature range characterizing the working conditions of low temperature ORC systems. Furthermore the majority of the published data result from refrigeration studies (Longo & Gasparella, 2007) (Longo, 2012) where the evaporating conditions are far away from the ones related to low temperature ORC systems. In order to fill the lack of experimental data and to validate two-phase evaporating correlations for low temperature ORC systems, a test-rig has been recently built at the Technical University of Denmark (DTU). The unit is equipped with seven BPHXs and it allows running experimental tests to characterize the thermal phenomena driving the vaporization and condensation of organic fluids in a wide temperatures and pressures range.

In this work the preliminary results of an experimental campaign investigating the vaporization of HFC-134a are presented. The fluid was tested at typical evaporating temperatures characterizing the working conditions of ORC power systems for low quality WHR applications. The refrigerant heat transfer coefficient and pressure drop were investigated for varying the average vapour quality in the evaporator. The article is organized as follow: section 2 describes the experimental facility available at DTU, while in section 3 the methodology to analyse the data is presented. The results are investigated in section 4 and the main conclusions are outlined in section 5.

2. EXPERIMENTAL SET UP

The process flow diagram and the front view of the heat exchanger (HX) test-rig are shown in Figure 1 and 2 respectively. The experimental rig includes three loops: the working fluid, the cooling water and the heating loop. The first

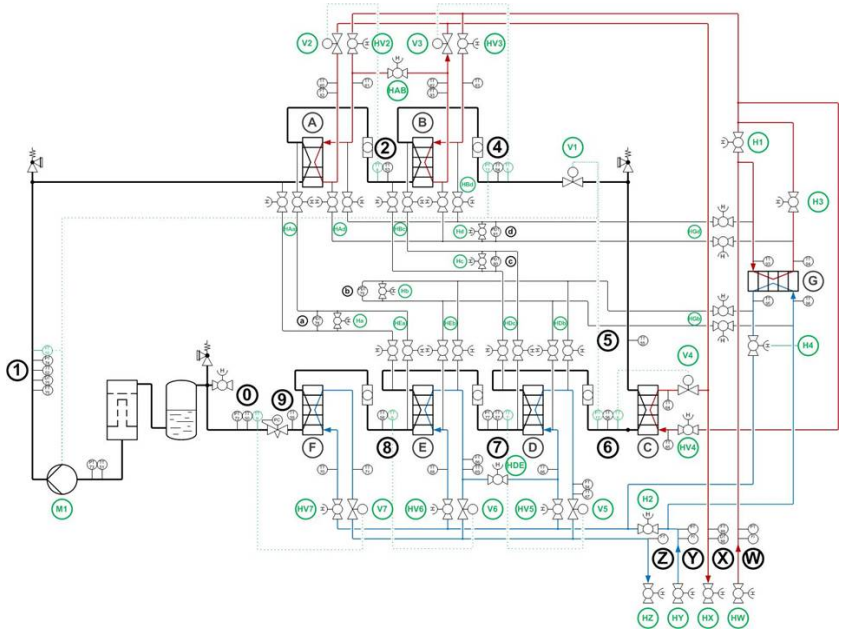

Figure 1: Process flow diagram of the HX test rig.

one is composed by 6 brazed plate heat exchangers connected in series. Referring to the bottom left side of figure 1, the working fluid is pumped through the pre-heater, HX-A, and the evaporator, HX-B, exiting in two-phase or superheated

condition. The fluid is then flashed through the expansion valve, V1, before entering the low pressure evaporator, HX-C, the de-superheater, HX-D, the condenser, HX-E, and the sub-cooler, HX-F. At the outlet of HX-F, the fluid in liquid state is stored in the receiver tank. A filter placed at the pump inlet protects the machine from any solid residues present in the fluid. The variable speed volumetric pump allowed controlling the working fluid flow rate. The evaporating pressure was regulated by the expansion valve, V1, the pump speed and the temperature and mass flow of the thermal oil. A seventh BPHX, HX-G, is installed on the set up. HX-G is used for Wilson-plot experiments (Shah, 1990) between the cooling water and the thermal oil.

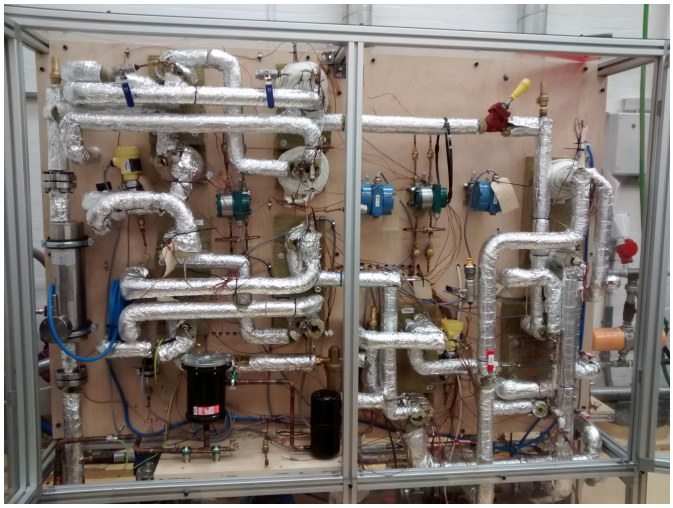

Figure 2: Front view of the HX test rig.

The cooling water circuit is a closed loop. The water rejects the thermal energy absorbed from HX-G,-D,-E,-F to the cooling network system via a brazed plate heat exchanger. Three automatic valves (V5-V6-V7)are used to adjust the water flow rate through HX-D,-E and-F, while five manually controlled valves give extra flexibility to the system allowing for different loop configurations (i.e. phase out one or more HXs or set the HXs in series or parallel). A volumetric pump, run at full speed, circulated water through the loop. The pressure is imposed by an expansion tank placed at the pump inlet.

In the third loop, thermal oil, Texatherm 22 (TX22) (CEPSA, 2016), is heated up in a tank by six electrical heaters and supplies thermal energy to HX-A,-B,-C and -G. A variable speed centrifugal pump circulated the oil through the loop. Three electronic valves (V2-V3-V4) installed at the outlet of HX-A,-B and-C allow controlling the oil mass flow rate, while six manual valves allow for different loop configurations.

Calibrated T-type thermocouples were used to measure the temperature of the working fluid, the cooling water and the thermal oil at the inlet and the outlet of each component. The working fluid pressure at the inlet of the pre-heater was measured by a pressure transmitter, whereas the refrigerant pressure drop through the evaporator was measured with a differential pressure sensor. The working fluid mass flow rate and density were measured at the pump outlet with a Coriolis flow meter. Two turbine volume flow meters were used to measure the oil volume flow at the outlet of HX-A and -B. A Coriolis flow meter installed on the return pipe from the test-rig to the oil tank measured the TX22 mass flow rate and density. The water volume flow rate was measured at HX-D and HX-E outlets by two magnetic volume flow meters. The uncertainty of the sensors are reported in Table 1. A PLC was used for basic control purposes and data acquisition was carried out with Labview. Thermodynamic calculations were performed in real-time via the CoolProp-Labwiew wrapper (Bell, Wronski, Quoilin, & Lemort, 2014).

The heat exchangers are of the brazed plate type. The pre-heater and evaporator consist of 8 and 10 plates respectively, 76 mm in width and 317 mm in length with an herringbone corrugation. The main geometrical characteristics of the BPHXs are reported in Table 2. During the experiments, the pre-heater, HX-A, and evaporator, HX-B, were connected in parallel on the secondary fluid side, and were fed with a varying thermal oil mass flow rate at a constant temperature. In order to bring the system in steady-state condition, in the cooling loop water was pumped to the inlet of HX-D,-E and -F with a constant mass flow rate and temperature. The system was considered in steady-state when the oscillations characterizing all the temperature readings exhibited an amplitude lower than 0.5 K for 120 seconds. Once this condition was reached, all the measures were recorded for 120 seconds and averaged over this time.

Table 1: Range and precision of the measurement devices. *k*: coverage factor. CFM: Coriolis flow meter. TFM: turbine flow meter. MFM: Magnetic flow meter. TC: Thermocouple. PT: pressure transmitter. DPS: differential pressure sensor.

Variable	Device type	Model	Range	Uncertainty (k=2)
$\dot{m}_{wf}$	CFM	Siemens 2100 DI6	0-0.15 kg s^{-1}	± 0.06%
$\dot{m}_{hf}$	CFM	Siemens 2100 DI15	0-0.8 kg s^{-1}	± 0.02 %
$\dot{V}_{hf}$	TFM	GL flow - LX13	2-20 l min^{-1}	± 0.1 %
$\dot{V}_{cf}$	MFM	Yokogawa RXF015G	0-20 l min^{-1}	± 1 %
T	TC	Omega Type T	20-180 °C	± 0.19 K
p	PT	Vegabar82	1-51 bar	± 0.45 %
Δp	DPS	Yokogawa EJX110A	5-400 mbar	± 0.038%

Table 2: Geometrical characteristics of the brazed plate used for the BPHXs. PROPIN: proprietary information.

Parameter	Symbol	Value
Total length (mm)	L_{tot}	314
Plate width (mm)	B_p	76
Port diameter (mm)	d_p	16
Plate thickness (mm)	l_p	0.3
Wave length (mm)	l_{co}	PROPIN
Corrugation depth (mm)	a_{co}	0.095
Corrugation type (-)		Herringbone
Area of the plate (m^2)	A_p	0.02329

3. DATA REDUCTION

In the evaporator, HX-B, the overall heat transfer coefficient U is equal to:

$$U = \frac{\dot{Q}}{A_{HX}\Delta T_{ln}} \tag{1}$$

where the thermal energy $\dot{Q}$ was calculated from the oil side of the heat exchanger as:

$$\dot{Q} = \dot{m}_{oil} \cdot (h_{oil,su} - h_{oil,ex}) \tag{2}$$

The heat transfer area, A_{HX} was computed as:

$$A_{HX} = A_p \cdot n_{ch,min} \cdot 2 \tag{3}$$

where $n_{ch,min}$ is the minimum number of channel between the two HX sides and A_p is the area of one plate calculated as shown in Equation 4:

$$A_p = L_{tot} \cdot B_p - \pi \cdot d_p^2 \tag{4}$$

As the refrigerant passed through the evaporator in two-phase flow with no phase transition, the logarithmic mean temperature difference was calculated as:

$$\Delta T_{ln} = \frac{T_{oil,su} - T_{oil,ex}}{ln\left(\frac{T_{oil,su} - T_{sat}}{T_{oil,ex} - T_{sat}}\right)} \tag{5}$$

where T_{sat} is the refrigerant saturation temperature at the evaporating pressure $p_{HXB,su}$. The average heat transfer coefficient of the refrigerant in HX-B was then computed as:

$$\alpha_{wf} = (1/U - R_{wall} - 1/\alpha_{oil})^{-1} \tag{6}$$

where R_{wall} is the metal wall thermal resistance defined as the ratio of the plate thickness, l_p, to the metal thermal conductivity, k_{wall}, computed at the wall average temperature $T_{wall,m}$ defined as:

$$T_{wall,m} = \frac{T_{oil,su} + T_{oil,ex} + T_{wf,su} + T_{wf,ex}}{4} \tag{7}$$

In order to solve Equation 6, the oil side heat transfer coefficient, α_{oil}, is required. A specific set of water-oil experiments based on the Wilson plot method were performed on HX-G to identify the oil heat transfer coefficient. In particular the modified Briggs and Young Wilson plot technique, described in (Shah, 1990), was adopted. A set of 20 steady-state points were identified leading to the following calibration correlation for the oil side heat transfer coefficient:

$$Nu = 0.274 \cdot Re^{0.8} \cdot Pr^{\frac{1}{3}} \cdot (\mu/\mu_{wall})^{0.14} \tag{8}$$

$$52 < Re < 205 \quad \Lambda \quad 76 < Pr < 105 \tag{9}$$

The working fluid vapour quality at the inlet, $X_{HXB,su}$, and outlet, $X_{HXB,ex}$, of the evaporator, HX-B, were calculated from the temperature and pressure at the inlet of the pre-heater, HX-A, adding the oil thermal energy exchanged in HX-A, $\dot{Q}_{HXA,oil}$ and HX-B, $\dot{Q}_{HXB,oil}$ as follow:

$$X_{HXB,su} = f(h_{HXB,su}, p_{HXB,su}) \tag{10}$$

$$h_{HXB,su} = h_{HXA,su} + \frac{\dot{Q}_{HXA,oil}}{\dot{m}_{wf}} \tag{11}$$

$$X_{HXB,ex} = f(h_{HXB,ex}, p_{HXB,ex}) \tag{12}$$

$$h_{HXB,ex} = h_{HXA,su} + \frac{\dot{Q}_{HXB,oil}}{\dot{m}_{wf}} \tag{13}$$

The frictional pressure drop during refrigerant vaporization, Δp_f, was evaluated based on the measured pressure drop subtracting the momentum, Δp_{mom}, the gravity, Δp_g and the manifolds and port, Δp_{mp}, pressure drops as explained in (Longo, 2012). For all the performed calculations the refrigerant properties were computed based on the open-source CoolProp library (Bell et al., 2014).

4. RESULTS AND ANALYSIS

Three sets of experimental data were collected at different saturation temperatures (60 , 70 and 80°C) for a total of 70 steady-state points. For each set, the working fluid was pre-heated in HX-A and entered the evaporator, HX-B, with the inlet vapour quality ranging between 0.01 and 0.3, while the outlet vapour quality conditions varied between 0.5 and 0.95. The refrigerant mass flow was kept constant at 0.075 kg.s^{-1}. In Table 3 the operating conditions of the evaporator during the experimental tests are reported. A detailed propagation error analysis was performed following the guidelines of (Kline & McClintock, 1953). A maximum uncertainty of 9.5% was found for the refrigerant heat transfer coefficient and of 5% for the pressure drop. In Table 4 the uncertainty values for the most relevant variables are listed.

In Figure 3, the refrigerant heat transfer coefficient, calculated based on Equation 6, is reported as a function of the

Table 3: Operating conditions in the evaporator HX-B during the experimental tests.

Fluid	runs	p_{eva} [bar]	X_{su}	X_{ex}	G_{oil} [kg s^{-1}m^{-2}]	$\dot{q}$ [kW m^{-2}]
R134a / HX-B	70	16.7-26.56	0.01-0.3	0.5-0.95	50.3 - 108.9	19.4 - 43.1

evaporator average quality X_m, defined in Equation 14, for the three analysed saturation temperatures.

$$X_m = \frac{X_{HXB,su} + X_{HXB,ex}}{2} \tag{14}$$

The flow boiling heat transfer coefficient slightly decreases with increasing mean vapour quality. This could be related by local occurrence of partial dry-out Similar results were found by (Shiferaw, Karayiannis, & Kenning, 2009) and

Table 4: Uncertainty of the main calculated variables for the evaporator.

Variables	Maximum uncertainty (k =2)
Geometrical parameters	
Area HX-B	± 0.0028 m^2
Heat transfer and pressure drop parameters	
Heat flow rate	-
Vapour quality	± 0.026
Overall heat transfer coefficient	± 2 %
Refrigerant heat transfer coefficient	± 9.5 %
Pressure drop	± 5 %

(Copetti, Macagnan, Zinani, & Kunsler, 2011). Furthermore the heat transfer coefficients show great sensitivity to saturation temperature contrary to what has been shown by (Longo, 2012) and in line with the results of (Lazarek & Black, 1982) and (Shiferaw et al., 2009). The increase in heat transfer coefficient with increasing saturation pressure could be related to faster bubble growth (Shiferaw et al., 2009). In fact as the pressure increases the bubble departure diameter decreases and the bubble departure frequency increases (Sharma, Lee, Harrison, Martin, & Krishina, 1996).

In order to determine the dominant heat transfer regime during vaporization the criterion proposed by Thonon et

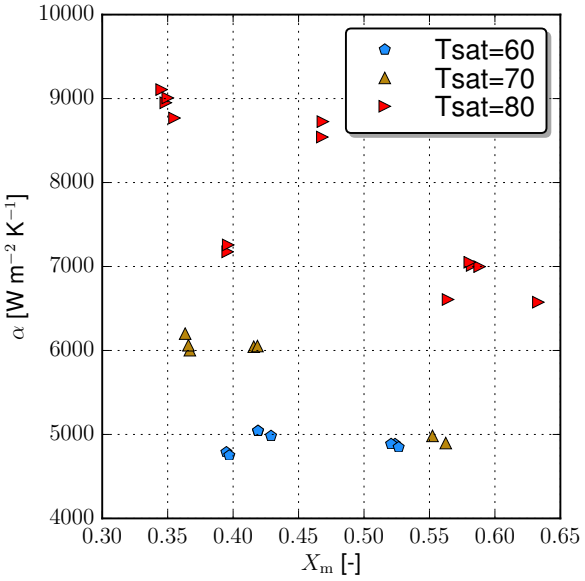

Figure 3: Variation of the boiling heat transfer coefficient versus the mean vapour quality for the three different saturation temperatures.

al. (Thonon, Vidil, & Marvillet, 1995) was applied. It is based on the product of the Boiling number , B_0, and the Lockart-Martinelli parameter, X_{tt}, and it is expressed as:

$$B_0 X_{tt} > 0.15 \cdot 10e^{-3} \quad \textit{Nucleate boiling regime} \tag{15}$$

$$B_0 X_{tt} < 0.15 \cdot 10e^{-3} \quad \textit{Convective boiling regime} \tag{16}$$

The results, shown in Figure 4a, highlight that all the measured steady-state points belong to the nucleate boiling regime. As a consequence the well-known Cooper correlation (Cooper, 1984) was used to predict the experimentally calculated heat transfer coefficients. The results are shown in figure 4b. As it is possible to see the correlation is able to predict the heat transfer coefficient values with an accuracy of 20 % for most of the collected experiments.

The frictional pressure drop is plotted versus the mean vapour quality in Figure 5. The two-phase frictional pressure

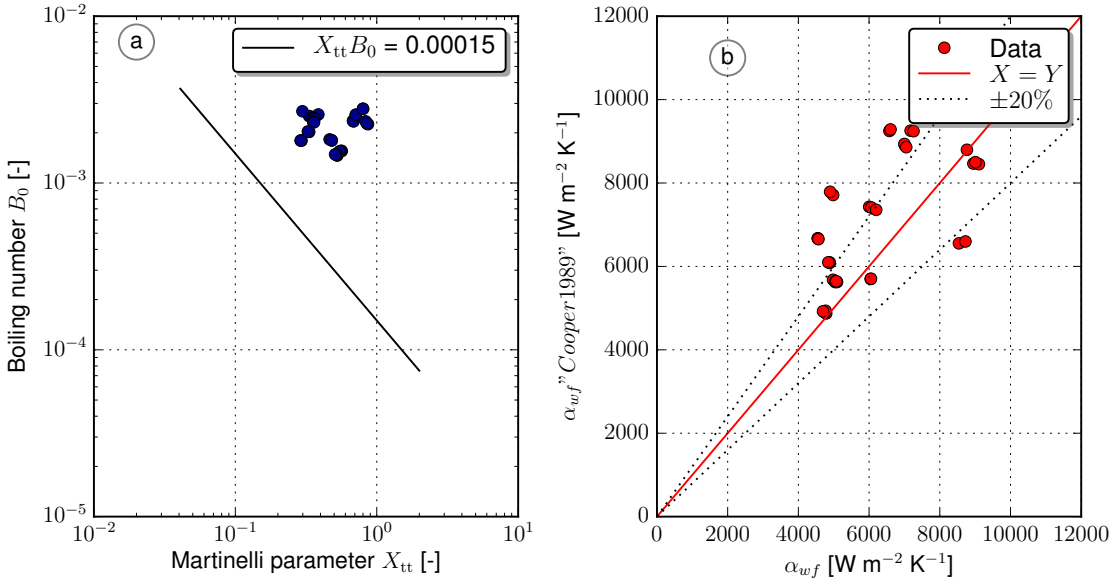

Figure 4: (a) Boiling heat transfer coefficient versus the Thonon et al. criterion. (b) Parity plot between experimental and calculated boiling heat transfer coefficient by Cooper et al.

drop is characterized by an increasing trend as the the mean vapour quality rises. This is due to the increase in the mass velocity of vapour. Furthermore the pressure drop decreases as the saturation pressure increases. This result can be explained by the change of thermo-physical properties, density and viscosity, with respect to the saturation temperature. In particular as pressure decreases, the liquid to vapour density ratio increases leading to higher frictional losses.

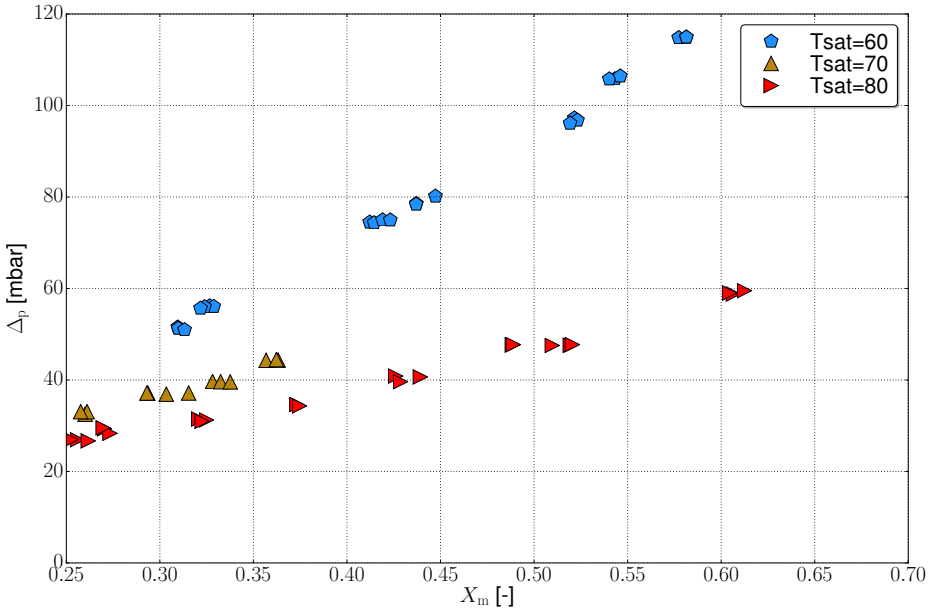

Figure 5: Frictional pressure drop versus mean vapour quality for different evaporating pressures.

5. CONCLUSIONS

This paper reports the first experimental results obtained on a test-rig installed at the Technical University of Denmark for studying heat transfer and pressure drop trends of organic fluids in small BPHXs. In particular the results of a preliminary experimental campaign to investigate the evaporation of refrigerant HFC-134a at high pressures are presented. The experimental results are reported in terms of refrigerant side heat transfer coefficient and frictional pressure drop. The effect of saturation temperature, inlet and outlet quality conditions on heat transfer and pressure drop during HFC-134a boiling inside BPHX was analysed. The main experimental findings are outlined hereunder:

- The heat transfer coefficient slightly decreases as the mean vapour quality increases especially for high saturation temperatures. These results are in line with the ones reported by (Shiferaw et al., 2009).
- Significant sensitivity of the heat transfer coefficients to saturation temperature is found.
- For the tested conditions, the Thonon criteria to identify the dominant heat transfer regime suggests that nucleate boiling has a major influence.
- The Cooper correlation (Cooper, 1984) predicts with a fairly good accuracy the experimentally calculated heat transfer coefficients.
- The pressure drop increases linearly with the increase of vapour quality and decreases with the increase of saturation temperature.

It is important to underline that the results presented in this contribution are preliminary findings. A more exhaustive experimental campaign covering the evaporation of R134a at high evaporating temperature investigating the effect of varying mass flux has been planned with the aim of validating the reported results.
Future work comprises the study of mixture vaporization and the investigation of brazed plate heat exchangers geometrical parameter on the performance of the evaporation process.

NOMENCLATURE

$\dot{m}$	Mass flow rate	($kg.s^{-1}$)
$\dot{V}$	Volume flow rate	($m^3.s^{-1}$)
T	Temperature	(°C)
p	Absolute pressure	(bar)
A	Area	(m^2)
$\dot{q}$	Heat flux	($W.m^{-2}$)
$\dot{Q}$	Heat flow	(W)
R	Thermal resistance	($m^2.K.W^{-1}$)
α	One side heat transfer coefficient	($W.m^{-2}.K^{-1}$)
Δ	Difference operator	(-)
U	Overall heat transfer coefficient	($W.m^{-2}.K^{-1}$)
μ	Viscosity	($kg.m^{-1}.s^{-1}$)
Subscript		
wf	working fluid	
su	supply	
ex	exit	
m	mean	

REFERENCES

Angelino, G., Bini, R., Bombarda, P., Gaia, M., Girardi, P., Lucchi, P., … Sabatelli, F. (1994). One MW binary cycle turbogenerator module made in europe.

Angelino, G., Gaia, M., & Macchi, E. (1984). A review of italian activity in the field of organic Rankine cycles. *Verein Deutscher Ingenieure Berichte 539*, 465-482.

Bell, I., Wronski, J., Quoilin, S., & Lemort, V. (2014). Pure- and pseudo-pure fluid thermophysical property evaluation and the open-source thermophysical property library CoolProp. *Industrial & Engineering Chemistry Research*, *53*, 2498–2508.

CEPSA. (2016, Accessed on 13 April). *http://www.cepsa.com/*.

Cooper, M. (1984). Heat Flow Rates in Saturated Nucleate Pool Boiling-A Wide-Ranging Examination Using Reduced Properties. *Advances in Heat Transfer*, *16*, 157–239. doi: 10.1016/S0065-2717(08)70205-3

Copetti, J. B., Macagnan, M. H., Zinani, F., & Kunsler, N. L. (2011, may). Flow boiling heat transfer and pressure drop of R-134a in a mini tube: an experimental investigation. *Experimental Thermal and Fluid Science*, *35*(4), 636–644. doi: 10.1016/j.expthermflusci.2010.12.013

Declaye, S., Quoilin, S., Guillaume, L., & Lemort, V. (2013). Experimental study on an open-drive scroll expander integrated into an ORC (organic Rankine cycle) system with R245fa as working fluid. *Energy*, *55*(0), 173 - 183. doi: http://dx.doi.org/10.1016/j.energy.2013.04.003

Desideri, A., B., D., Wronksi, J., Gusev, S., v. d. Broek, M., Lemort, V., & Quoilin, S. (2016). Comparison of moving boundary and Finite-Volume heat exchanger models in the Modelica language. *energies (accepted for publications)*.

IEA. (2010). *Industrial Excess Heat Recovery Technologies & Applications* (Tech. Rep.). Industrial Energy-related Technologies and Systems (IETS).

Kline, S., & McClintock, F. (1953). Describing uncertainties in single sample experiments.pdf. *Mechanical Engineering*.

Lazarek, G., & Black, S. (1982, jul). Evaporative heat transfer, pressure drop and critical heat flux in a small vertical tube with R-113. *International Journal of Heat and Mass Transfer*, *25*(7), 945–960. doi: 10.1016/0017-9310(82)90070-9

Longo, G. a. (2012). Hydrocarbon Refrigerant Vaporization Inside a Brazed Plate Heat Exchanger. *Journal of Heat Transfer*, *134*(10), 101801. doi: 10.1115/1.4006817

Longo, G. a., & Gasparella, a. (2007). Heat transfer and pressure drop during HFC refrigerant vaporisation inside a brazed plate heat exchanger. *International Journal of Heat and Mass Transfer*, *50*(25-26), 5194–5203. doi: 10.1016/j.ijheatmasstransfer.2007.07.001

Muley, a., & Manglik, R. M. (1999). Experimental Study of Turbulent Flow Heat Transfer and Pressure Drop in a Plate Heat Exchanger With Chevron Plates. *Journal of Heat Transfer*, *121*(1), 110. doi: 10.1115/1.2825923

Palm, B., & Claesson, J. (2006). Plate Heat Exchangers: Calculation Methods for Singleand Two-Phase Flow. *Heat Transfer Engineering*, *27*(4), 88–98. doi: 10.1080/01457630500523949

Prasad, A. (1980). Power generation from waste heat using organic rankine cycle systems. In *Proceedings from the second industrial energy technology conference houston, tx.*

Quoilin, S. (October 2011). *Sustainable energy conversion through the use of organic rankine cycles for waste heat recovery and solar applications* (Unpublished doctoral dissertation). University of Liege.

Quoilin, S., van den Broek, M., Declaye, S., Dewallef, P., & Lemort, V. (2013). Techno-economic survey of organic Rankine cycle ORC systems. *Renewable and Sustainable Energy Reviews*, *22*, 168-186. doi: 10.1016/j.rser.2013.01.028

Shah, R. K. (1990). Assessment of modified wilson plot techniques for obtaining heat exchanger design data. In *The ninth international heat transfer conference.*

Sharma, P., Lee, A., Harrison, T., Martin, E., & Krishina, N. (1996). *Effect of pressure and heat flux on bubble departure diameters and bubble emission frequency* (Tech. Rep.). Grambling State University.

Shiferaw, D., Karayiannis, T., & Kenning, D. (2009, feb). Flow boiling in a 1.1 mm tube with R134a: Experimental results and comparison with model. *International Journal of Thermal Sciences*, *48*(2), 331–341. doi: 10.1016/j.ijthermalsci.2008.02.009

Thonon, B., Vidil, R., & Marvillet, C. (1995). Recent research and developments in Plate Heat Exchangers. *Journal of Enhanced heat transfer*, *2*, 149–155.

Verneau, A. (1979). Waste heat recovery by organic fluid Rankine cycle. In *Proceedings from the first industrial energy technology conference houston.*

Walraven, L. B., D., & D haeseleer, W. (2013). Comparison of thermodynamic cycles for power production from low-temperature geothermal heat sources. *Energy Conversion and Management*, *66*(0), 220 - 233. doi: http://dx.doi.org/10.1016/j.enconman.2012.10.003